

PAPER

Measurement of small molecule diffusion with an optofluidic silicon chip†

Cite this: *Lab Chip*, 2013, 13, 4392

Eva Ryckeboer,^{*ab} Jan Vierendeels,^c Agnes Lee,^{ab} Sam Werquin,^{ab} Peter Bienstman^{ab} and Roel Baets^{ab}

In this work we explore the micro-ring resonator platform to study the diffusion-driven mass transport of small molecules within microfluidic channels. The micro-ring resonators are integrated on a silicon-on-insulator photonic chip and combined with microfluidics in poly(dimethylsiloxane) (PDMS). We apply a strong initial gradient in the solute concentration and use the micro-ring resonators to observe how this concentration evolves over time and space. This can be achieved by tracking the optical resonances of multiple micro-rings as they shift with changing solute concentration. Experiments are performed for both glucose and NaCl and at different temperatures. The measured concentration profiles are used to calculate the diffusion coefficient of both glucose and NaCl in water. The good agreement between measurement and theoretical prediction demonstrates the relevance of this method.

Received 24th June 2013,
Accepted 23rd August 2013

DOI: 10.1039/c3lc50752a

www.rsc.org/loc

1. Introduction

During the past decade microfluidics has emerged as an attractive platform to study bio-chemical processes on a small scale. For many applications, the mass transport in the microfluidic channels needs to be controlled and monitored accurately. Molecular diffusion plays an important role in this mass transport and therefore it is often required to study the diffusion of a particular molecule. This can be achieved with multiple methods, *e.g.* interferometry^{1,2} or fluorescence microscopy.^{3,4} Typical limitations include the stability requirements for an interferometric set-up and a need for labeling and a limited field-of-view of the microscope for the latter method. It is, however, true that there is no diffusion-measurement technique that outperforms all other techniques. Therefore, the preferred method is often a choice based on the availability of equipment, cost and microfluidic chip layout. In this work we present a straightforward method to investigate diffusion-driven mass transport in microfluidic channels with an integrated optofluidic device. We take advantage of the successful micro-ring resonator platform that brought about various demonstrations of

real-time sample analysis with concentration accuracies down to 10 ng mL⁻¹ and as low as 60 fM when receptor molecules are used.^{5,6} A micro-ring resonator is a resonant device in which the resonant optical frequencies depend on the refractive index of the surrounding fluid. The refractive index of the fluid alters with changing concentration of its solutes and their refractive indices. We use ring resonators that are integrated on a silicon-on-insulator (SOI) chip using standard CMOS processing. This offers three important advantages. First of all, these ring resonators allow for very sensitive measurements of small changes in the refractive index due to their high quality factor. Secondly, they can be multiplexed given their small size. Thirdly, the SOI chips can be mass-fabricated, resulting in a low cost sensor. The SOI chip is combined with microfluidic channels in poly(dimethylsiloxane) (PDMS). The microfluidic channels are fabricated using soft lithography.⁷ The determining microfluidic channel, utilized to observe diffusion, encloses a set of equally spaced micro-ring resonators. This channel is open on one side for the solute to enter, but is closed on the other side so as to avoid flow. We apply a step function in solute concentration at the entrance of this channel and observe how the concentration evolves along the channel. As the channel is long but narrow, we essentially study the longitudinal diffusion. The concentration profile is measured at the discrete positions of the microring resonators but continuously over time. We performed experiments with both glucose and NaCl as example molecules. For the glucose experiments we investigated the influence of flow perpendicular to the entrance of the diffusion channel. For the NaCl experiments we verified the temperature-dependence of the diffusion coefficient. A straightforward

^a Photonics Research Group, Department of Information Technology, Ghent University-imec, St.-Pietersnieuwstraat 41, Ghent B-9000, Belgium. E-mail: eva.ryckeboer@intec.ugent.be; Tel: +32 9 264 8933

^b Center for Nano- and Biophotonics (NB-Photonics), Ghent University, Ghent B-9000, Belgium

^c Department of Flow, Heat and Combustion Mechanics, Ghent University, St.-Pietersnieuwstraat 41, Ghent B-9000, Belgium

† Electronic supplementary information (ESI) available: Measurements of the glucose and NaCl sensitivity measurements. See DOI: 10.1039/c3lc50752a

analysis based on the discretized 1D diffusion equation is used to extract the diffusion coefficient from the measurements. The resulting diffusion coefficients are in good agreement with their literature values. Important to notice is that no fluorescent labeling is required and that the proposed method can be employed for any given molecule and transparent sample fluid as long as the solute concentration changes the refractive index of the sample fluid in a linear way. Other advantages include the large area of operation as the ring resonator sensors can be placed at any given position in the microfluidic channels. Another interesting feature is that reference sensors can be employed that monitor the temperature of the optofluidic chip during the experiments. In addition, it is a self-referenced method as the exact applied solute concentration at the entrance of the diffusion channel does not have to be known in order to calculate the diffusion coefficient.

The remainder of this paper is structured as follows: first, we review the micro-ring resonators platform for bio-sensing. Secondly, we discuss the measurement set-up and microfluidic design. We then present the experimental results and discuss the developed diffusion coefficient extraction method and its accuracy. Finally, we present the conclusion and future outlook.

2. Silicon-on-insulator micro-ring resonator sensing

2.1 Sensing principle

A silicon-on-insulator (SOI) ring resonator supports optical modes with wavelength λ that satisfy the resonance conditions

$$\frac{2\pi}{\lambda} n_{\text{eff}}(\lambda)L = m \cdot 2\pi \quad (1)$$

with n_{eff} the effective refractive index of the circulating mode, L the circumference of the ring and m is an integer representing the order of resonance. From this relation and in the absence of dispersion, it follows that a change in the effective refractive index leads to a shift in the resonant wavelengths:

$$\Delta\lambda = \frac{\Delta n_{\text{eff}} L}{m} \quad (2)$$

By taking the transmission spectrum of a ring resonator and by subsequently identifying the wavelength shift of the resonances, one can thus detect a change in the surrounding fluid. In an aqueous solution, the refractive index changes linearly with the solute concentration. For glucose *e.g.* the proportionality constant is 2×10^{-5} change in refractive index unit (RIU) per mmol.⁸ A micro-ring is thus readily implemented as a glucose sensor. Fig. 1 demonstrates how the transmission spectrum of a micro-ring changes when glucose is present.

However, it is useful to rewrite eqn (2) to take into account dispersion, which is large for the high-index contrast SOI material system. Due to dispersion, the resonance

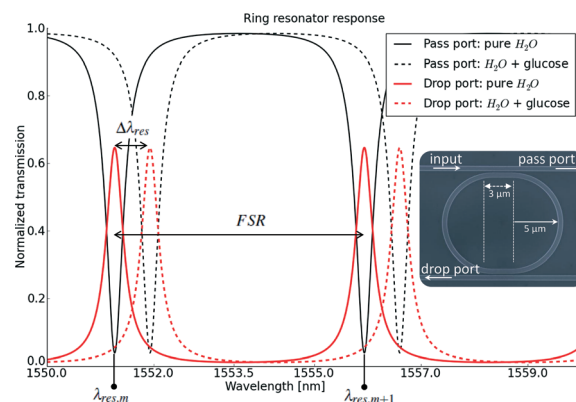


Fig. 1 Simulation of the transmission spectrum of a micro-ring resonator in add-drop configuration. The red and black curves show respectively the drop and pass ports. The resonant wavelengths shift due to the presence of glucose with a concentration of 50 mmol.

wavelength change will also have an effect on n_{eff} . The resulting equation given first order dispersion is:⁹

$$\Delta\lambda_{\text{res}} = \frac{\Delta n_{\text{env}} n_{\text{eff}} \cdot \lambda_{\text{res}}}{n_{\text{g}}} \quad (3)$$

in which $\Delta n_{\text{env}} n_{\text{eff}} = \left(\frac{\partial n_{\text{eff}}}{\partial n_{\text{env}}} \right)_{\lambda=\lambda_{\text{res}}} \Delta n_{\text{env}}$ with Δn_{env} the change in refractive index in the environment and n_{g} is the group index, defined as $n_{\text{g}} = n_{\text{eff}} - \lambda \frac{\partial n_{\text{eff}}}{\partial \lambda}$.

2.2 Silicon-on-insulator design

The photonic chip is fabricated in a CMOS pilot line on a 200 mm SOI wafer, comprising a 220 nm thick Si waveguide layer on a 2 μm buried oxide layer.¹⁰ The waveguides are 500 nm wide and 220 nm high and we only excite the transverse-electric (TE) mode of the waveguide. The ring resonators have a footprint of $12 \times 12 \mu\text{m}^2$ and are grouped in sets of four rings with slightly increasing circumference. These four rings are in the add-drop configuration (see Fig. 1) and spaced equally with a distance of 1.8 mm. At the operating wavelength of 1550 nm, the free spectral range of the rings with water cladding is around $\text{FSR} = \frac{\lambda^2}{n_{\text{g}} L} = 16.4 \text{ nm}$

3. Experimental set-up

3.1 Optical read-out system

All micro-rings are fed by one tunable laser source. The laser light is coupled from an optical fiber into the SOI chip using grating couplers.¹¹ Identical grating couplers are used to image the signal from both the pass and drop ports of all the ring resonators simultaneously onto a fast infrared camera. By tuning the laser wavelength, the output spots from the drop ports will vary in intensity with peaks at the ring resonances. Conversely, the pass ports will show a dip in intensity at the ring resonances. More details on the optical set-up can be found in ref. 12.† The optofluidic chip is

mounted on a temperature controller and the experiments took place in a cleanroom environment. The data acquisition rate to measure consecutive transmission spectra depends on the FSR of the set of micro-rings and the chosen wavelength resolution to resolve the various resonances. It takes *e.g.* 16 seconds to measure the transmission spectrum over a wavelength range of 16 nm with a stepped resolution of 10 pm. The transmission spectra are continuously acquired. For every transmission spectrum, we first fit a Lorentzian to the resonance to determine the peak wavelength. This way we can accurately determine the wavelength shift of the resonances between consecutive measurements. In our set-up, the smallest detectable wavelength is 0.6 pm, which corresponds to a glucose concentration of 0.079 g L^{-1} and to a NaCl concentration of 0.066 g L^{-1} .

3.2 Microfluidics design and fabrication

The microfluidics are fabricated in poly(dimethylsiloxane) (PDMS) (Sylgard[®] 184, Dow Corning Corporation) using soft lithography.⁷ The fluidic channels are $200 \mu\text{m}$ wide and $50 \mu\text{m}$ high. Both the SOI-chip and PDMS are given a short oxygen-plasma treatment before applying direct bonding with a flip-chip machine.¹³ The microfluidic design has one main channel connecting the inlet with the outlet and one perpendicular branch which we call the diffusion channel. The diffusion channel must be closed at one side to avoid flow in this branch. This raises a practical issue as initially the diffusion channel has to be filled with water. The easy solution to this is to punch a small hole such that water can enter the diffusion channel and then seal this hole for the remainder of the experiments. Two slightly different designs were fabricated, differing mainly in the number of ring resonators that are enclosed. The first design is shown in Fig. 2(a) and was used for the glucose diffusion experiments. The small number of bends in this design is interesting to study the effect of flow in the main channel but limits the number of micro-rings that are sampled. The second design (Fig. 2(b)) encloses four sets of micro-rings with a spacing of 1.8 mm. Each set has three vertically spaced ring resonators separated by a short distance of 0.1 mm. This design was used for the NaCl diffusion experiments.

3.3 Fluid handling

Deionized (DI) water solutions with glucose concentrations of respectively 70 g L^{-1} , 90 g L^{-1} , and 300 g L^{-1} (D-glucose from Sigma-Aldrich) were prepared as well as a NaCl solution with a concentration of 300 g L^{-1} . To avoid air bubbles in the solutions, they are degassed in an ultrasonic bath with a vacuum pump. This step is very important as the change in refractive index between water and air gives a huge shift in resonance wavelengths and distorts the measurement results heavily. To switch between two solutions without generating an air bubble, we use a valve. A syringe injection pump (Harvard apparatus) is used to pump the pure DI water sample fluid to the valve and the sample loop contains the glucose or NaCl

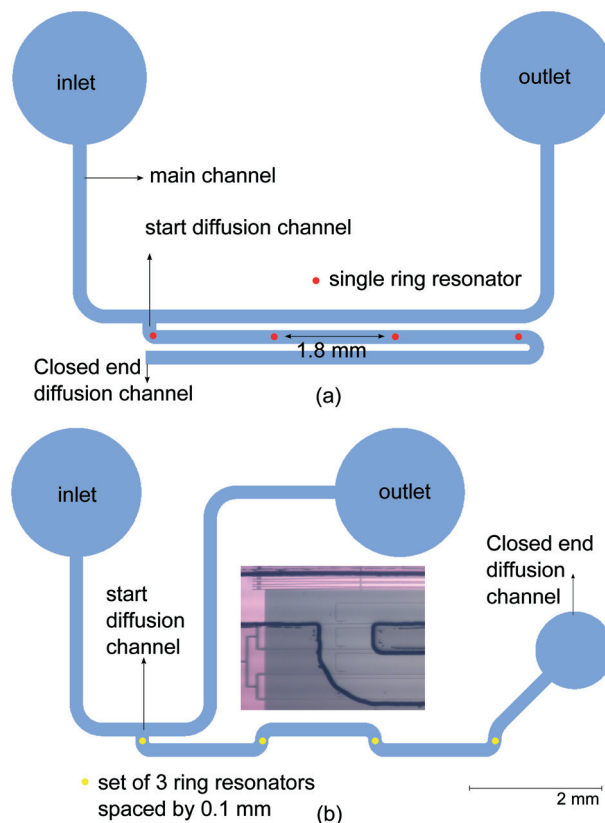


Fig. 2 (a) Microfluidics design showing the main channel, from inlet to outlet, and the perpendicular diffusion channel, that encloses the ring resonator sensors. (b) Microfluidics design that is used for NaCl experiments. The diffusion channel contains four times a set of three closely spaced micro-rings.

solution. The output of the valve is connected to the inlet of the PDMS microfluidics with a flexible PTFE micro-tube. The outlet is connected with a similar tube to a petri dish to collect the waste fluids.

4. Glucose diffusion experiments

We first experimentally verified the expected wavelength shift for a glucose concentration of 300 g L^{-1} . We then performed two experiments, one with flow and one with stopped flow in the main microfluidic channel. This way we can study the effect of the flow in the flow channel on the speed of mass transport in the diffusion channel at the set temperature of $25 \text{ }^\circ\text{C}$.

4.1 Measurement of the glucose induced resonance shift

To measure the sensitivity of the ring resonators for glucose, we evaluate the shift in resonance of the ring resonators due to a glucose concentration of 300 g L^{-1} . A straight microfluidic channel is placed above a set of 7 ring resonators and a set of three ring resonators is positioned just outside this microfluidic channel to serve as a reference. First, pure DI water is applied, followed by a glucose solution of 300 g L^{-1} . After about 3 minutes the valve is switched back to pure DI water. The ring resonators inside the microfluidic channel

experience a mean wavelength shift of 2.44 nm after 150 seconds whereas the reference resonators show the expected flat response.† Although the ring resonators are identical in design, the fabrication process leads to small differences in the physical dimensions of the ring resonators. This causes each of them to have a slightly different sensitivity, hence resonance shift, for glucose. The standard deviation on the mean shift is 12.7 pm which corresponds to a 0.5% variation between the different micro-rings.

4.2 Experiment with stopped flow

Initially we flow the pure DI solution through the main channel of the optofluidic chip. The pump speed is set to $10 \mu\text{L min}^{-1}$. The flow is laminar given the dimensions of the microfluidic channels. There is no flow in the diffusion channel as it is completely sealed as explained in section 3.1. We then switch the valve to the glucose solution of 90 g L^{-1} and inspect the transmission spectrum of the first ring which is at the entrance of the diffusion channel. As soon as the resonances of this ring start to shift, the pump is switched off. This makes sure that the main channel now serves as a still glucose reservoir (but with a slowly time-varying concentration). During the fluid transfer from valve to optofluidic chip, a parabolic flow profile in the 25 cm long PTFE micro-tube leads to a strong radial concentration gradient. This leads to a large diffusion component in the radial direction and reduces the mean axial concentration gradient in the downstream flow direction. Thus, given that diffusion also occurs in the 25 cm long PTFE micro-tube, there is no sharp transition between the water and glucose solution. Therefore, when the first ring starts to shift, the concentration in the main channel is not immediately 90 g L^{-1} . In our experiment, the concentration in the main channel is 60 g L^{-1} when the pump is stopped. The glucose concentration at each ring is monitored

for about two hours to observe the diffusion process. The measurement results are presented in Fig. 3(a).

It shows the expected outcome that the first ring, at a distance of $145 \mu\text{m}$ from the main channel, reacts fast to the sudden concentration gradient and soon reaches saturation. The rings at distances $1945 \mu\text{m}$ and $3745 \mu\text{m}$ show a delayed and slower rise. The last ring at $5545 \mu\text{m}$ is used as a temperature reference for the ring responses of the three other rings. To gain insight into the concentration profiles, we simulated the step response with the computational flow dynamics (CFD) software ANSYS Fluent®. The simulated glucose distribution is also shown in Fig. 3(a). The designed geometry of the microfluidics and inlet tube is used and the Navier–Stokes equations for incompressible fluids are solved. The literature value of the glucose diffusion coefficient $6.7 \times 10^{-10} \text{ m}^2 \text{ s}^{-1}$ at $25 \text{ }^\circ\text{C}$ is used.¹⁴ We also include the effect of glucose diffusion in the 25 cm long PTFE micro-tube, leading to the main microfluidic channel. We can see a close agreement between the simulations and the experimental data. The main differences are caused by the amount of mixing of glucose and water during the flow section, which cannot be properly predicted when the designed geometry rather than the fabricated geometry is used. In the later section 6 we calculate the glucose diffusion coefficient based on these measurements.

4.3 Experiment with flow

Throughout the complete second experiment, we pump the fluids with a steady flow of $10 \mu\text{L min}^{-1}$. Again, we verify that there is no flow in the diffusion channel. At first, the channels are filled with pure DI water, then the valve is switched to a glucose solution of 70 g L^{-1} . After 50 minutes the valve is switched back to the pure DI solution. The ring resonator responses to this applied block function are shown in Fig. 3(b). As the pump is running continuously, there is a constant

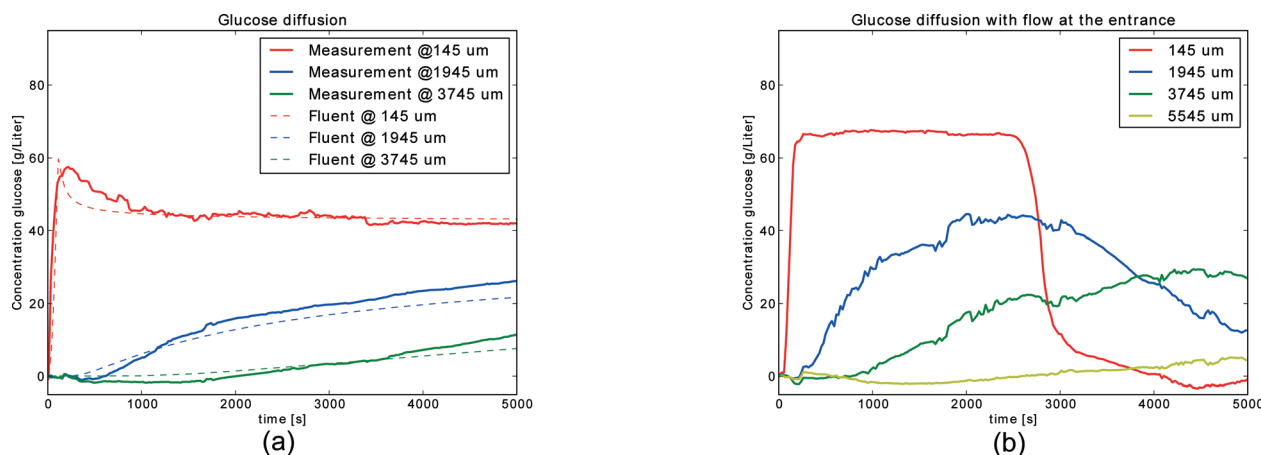


Fig. 3 Glucose concentration as calculated from the wavelength shift of the micro-ring resonances as a function of time at the discrete positions of the ring resonators for both (a) stopped flow and (b) continuous flow at the entrance of the diffusion channel. The wavelength shifts are a direct measure for the position and time-dependent glucose concentration in the diffusion channel. Full line: measurement, dotted line: simulation.

supply of glucose molecules with a fixed concentration to the entrance of the diffusion channel.

The signal from the first ring corresponds well with the applied glucose concentration profile. The second and third ring both show the increase and decrease in glucose concentration whereas the decrease still has to set in for the last ring. When we compare the time scale of the experiment with and without stopped flow, we immediately note the faster mass transport of the latter. If we look *e.g.* at the response of the ring resonator at a distance of 1945 μm from the entrance of the diffusion channel, we note that it has reached a glucose concentration of 43.7 g L^{-1} after 2500 seconds in the case of continuous flow at the entrance whereas it only reaches 17.7 g L^{-1} when the flow was stopped. The applied input concentration, however, was respectively 70 g L^{-1} and 60 g L^{-1} . This faster mass transport can be explained by two effects. Firstly, the main channel serves as a reservoir with constant concentration and secondly, the presence of a convective flow that carries the glucose molecules down the diffusion channel. Although the diffusion channel is closed, the flow in the main channel induces convective currents. This is an example of a driven cavity which is a well-known phenomenon in viscous incompressible fluids.^{15,16} The velocity of the convective flows decreases exponentially along the diffusion channel. In more details: the simulated convective flow velocity is 1 $\mu\text{m s}^{-1}$ at a distance of 200 μm from the entrance of the diffusion channel while at a distance of 1 mm this velocity is already reduced to 1 pm s^{-1} . This makes the effect of faster mass transport much stronger at the second ring than at the third.

5. NaCl diffusion experiments

Three experiments with NaCl were performed. In the first experiment we detect the sensitivity of the ring resonators to NaCl. In the second and third experiment we perform a diffusion experiment with stopped flow at both 20 °C and 30 °C. This allows us to confirm the faster diffusion rate with increasing temperature.

5.1 Sensitivity to NaCl

In the first experiment we determine the sensitivity of the micro-ring resonators to a 300 g L^{-1} NaCl aqueous solution. The pump speed is set to 25 $\mu\text{L min}^{-1}$. First pure DI water is applied, followed by the NaCl solution after which we switch the valve again to pure DI water. The resulting evolution of the resonance shift for a set of seven ring resonators is measured.† The three reference ring resonators that are outside the microfluidic channel show a flat response. The micro-ring resonators exhibit a mean shift of 2.71 nm after 500 seconds with a standard deviation of 46 pm. This corresponds to a 1.7% variation between the different rings with an identical design. This is a rather high value but poses no problem to accurately study the evolution of concentration profiles in micro-fluidic channels. Indeed, the information from this type of measurement can be used to our advantage to calibrate the response from the individual micro-ring resonators. First a sensitivity factor $\frac{\Delta\lambda_{\text{ring}}}{\Delta\lambda_{\text{mean}}}$ is calculated for each ring with $\Delta\lambda$ the wavelength shift due to 300 g L^{-1} of NaCl. This sensitivity factor is then used to linearly scale the measured resonance shift during the diffusion experiments. In addition, the mean shift is used to calculate the conversion factor between wavelength shift [nm] and NaCl concentration [g L^{-1}].

5.2 Experiment at 20 °C

Initially we flow the pure DI solution through the main channel of the optofluidic chip. The pump speed is set to 5 $\mu\text{L min}^{-1}$ and the temperature controller is fixed at 20 °C. We then switch to the NaCl solution and as soon as the first ring resonator starts to shift the pump is stopped. The shift of the ring resonators is then recorded during 2500 seconds. The results are shown in Fig. 4(a). The time axis starts at the transition from pure DI water to the NaCl solution. The stated position of the various ring resonators is the distance from the entrance of the diffusion channel to the ring resonator (as designed), with straight lines and 90 degree bends, along the center line of the microfluidic channel.

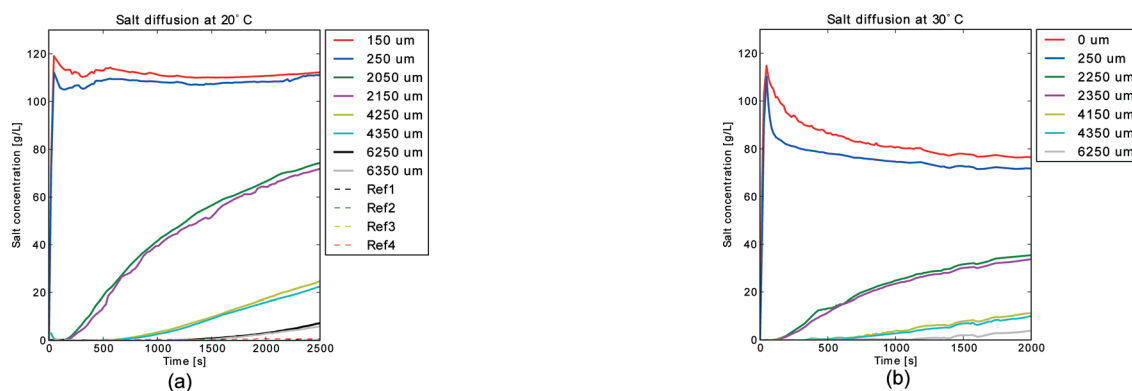


Fig. 4 NaCl concentration as calculated from the wavelength shift of the micro-ring resonances as a function of time at the discrete positions of the ring resonators (a) at a temperature of 20 °C and (b) at a temperature of 30 °C. The dotted lines show the flat responses of the reference ring resonators.

5.3 Experiment at 30 °C

For this experiment, a new optofluidic chip was fabricated. The temperature controller was set to 30 °C and the flow speed to 5 $\mu\text{L min}^{-1}$. After switching to the NaCl solution from a pure DI solution, the pump was stopped when the first ring resonator is shifting in resonance. The results of this measurement are shown in Fig. 4(b). Again a clear diffusion profile is found.

6. Extraction of the diffusion coefficient

To calculate the diffusion coefficient D , we use the explicit finite difference expression of the 1D diffusion equation:

$$\frac{C_{i+1,j} - C_{i,j}}{\Delta t} = \frac{D}{(\Delta x)^2} (C_{i,j+1} - 2C_{i,j} + C_{i,j-1}) \quad (4)$$

In the above equation, $C_{i,j}$ represents the solute concentration at time $t = i \cdot \Delta t$ and position $x = j \cdot \Delta x$. The microfluidic channel is approximated by a straight line of length 1 cm. The left boundary condition is a measured concentration profile C_{input} , whereas the right boundary condition is the impermeable wall condition. First, we set the step size along the microfluidic channel to Δx . We then perform a spline interpolation of the measured C_{input} to a fixed temporal grid with a time step Δt . To obey the stability condition for the explicit finite difference expression, this Δt must obey $\Delta t \leq \frac{\Delta x^2}{2D}$. Secondly, the evolution of solute concentration, during the experimental time of T_{exp} , is determined for a large set of diffusion coefficients along the microfluidic channel with step Δx . These theoretical curves $C_{i,j}(D)$ are then evaluated at the position of the ring that we want to predict. Finally, the sum of least squares $S(D)$ is calculated (eqn (5)) between these theoretically predicted $C_{\text{p}}(t, D)$ curves and the experimental results $C_{\text{exp}}(t)$ of the ring at a distance L .

$$S(D) = \sum_{t=0}^{t_{\text{exp}}} (C_{\text{exp}}(t) - C_{\text{p}}(t, D))^2 \quad (5)$$

We can then extract the measured diffusion coefficient as the minimum in the least squares curve $S(D)$. Important to note is that we use the raw concentration data from the measurements, without any post-processing such as noise filtering, as an input for the diffusion extraction procedure. The distance L , the shortest distance between the two rings, is determined by the microscope images from the fabricated sample. This is necessary as the fabricated sample can have a misalignment between the microfluidics and SOI design. The choice about which ring resonator serves as the input for the simulation C_{input} and which ring as the predicted curve C_{exp} can be optimized. Firstly, the input ring has to be closer to the entrance of the diffusion channel than the predicted ring. Secondly, the ring resonators close to the entrance of the diffusion channel can be influenced by the initial flow conditions whereas the ring resonators at the end of the diffusion channel have a weaker signal. In the NaCl experiment at 20 °C, we used the middle ring of set 2 to

predict the middle ring of set 3. The distance to the predicted ring is discretized into 100 parts, leading to $\Delta x = 19.45 \mu\text{m}$. The other parameters for the data analysis were $\Delta t = 0.1 \text{ s}$, $T_{\text{exp}} = 2500 \text{ s}$ and $L = 1945 \mu\text{m}$. The minimum in the least squares curve is found for a diffusion coefficient of $13.74 \times 10^{-10} \text{ m}^2 \text{ s}^{-1}$. For the NaCl experiment at 30 °C, the first ring of set 2 and the first ring of set 3 is used. They are horizontally aligned, therefore the distance L is $1800 \mu\text{m}$. The position step is $\Delta x = 18 \mu\text{m}$, the time step $\Delta t = 0.09 \text{ s}$ and the total experimental time $T_{\text{exp}} = 1999.98 \text{ s}$. From the least squares fitting, we can extract a diffusion coefficient of $16.31 \times 10^{-10} \text{ m}^2 \text{ s}^{-1}$. Finally, we also extracted the glucose diffusion coefficient from the stopped flow experiment in section 2 using the rings at 1945 and 3745 μm with parameters $\Delta x = 18 \mu\text{m}$, $\Delta t = 0.2 \text{ s}$, $T_{\text{exp}} = 5000 \text{ s}$ and $L = 1800 \mu\text{m}$. A value of $6.55 \times 10^{-10} \text{ m}^2 \text{ s}^{-1}$ is obtained. We also investigated if a smaller Δx and Δt had an effect on the resulting diffusion coefficient. Hereto, we followed the same diffusion extraction procedure for the NaCl experiment at 30 °C with $\Delta x = 5 \mu\text{m}$, $\Delta t = 0.007 \text{ s}$ and $\Delta x = 10 \mu\text{m}$, $\Delta t = 0.025 \text{ s}$. We found that the diffusion coefficient equals $16.311 \times 10^{-10} \text{ m}^2 \text{ s}^{-1}$ for both $\Delta x = 5 \mu\text{m}$, $\Delta x = 10 \mu\text{m}$ and $\Delta x = 18 \mu\text{m}$, showing that the extracted diffusion coefficient varies less than 0.1%, hence, the numerical solution is converged. A clear advantage of this analysis method is that the exact concentration at the entrance of the diffusion channels does not have to be known. This entrance concentration is hard to predict and depends strongly on the exact experimental settings such as the length of the tubing, flow speed, connection between tubing and the microfluidics *etc.*

7. Discussion of the results

The measured concentration profiles are impacted by errors in the resonance fitting procedure, non-homogeneities in the sample fluid, and a limited acquisition rate. It is therefore interesting to evaluate how tight a diffusion estimate can be obtained. From the literature we find a NaCl diffusion coefficient of $13.08 \times 10^{-10} \text{ m}^2 \text{ s}^{-1}$ at 20 °C. This diffusion coefficient D was calculated from the literature value at 25 °C ($T_0 = 298.15 \text{ K}$) by using eqn (6) with μ the dynamic viscosity and T the temperature in kelvin.^{17,18}

$$D(T) = \frac{T \cdot \mu(T_0)}{T_0 \cdot \mu(T)} \cdot D(T_0) \quad (6)$$

Similarly, we find a NaCl diffusion coefficient of $16.79 \times 10^{-10} \text{ m}^2 \text{ s}^{-1}$ at 30 °C. The literature value of the glucose diffusion coefficient is $6.75 \times 10^{-10} \text{ m}^2 \text{ s}^{-1}$ at 25 °C.¹⁴ When we compare the diffusion coefficients obtained by the experiments and the literature values we find a discrepancy of -2.96% , $+5.04\%$ and -2.86% for glucose, NaCl at 20 °C and 30 °C respectively. To estimate the robustness of our method, we take a closer look at the NaCl experiment at 30 °C. First, the concentration profiles of both ring resonators (C_A and C_B), which were used to calculate the diffusion coefficient, are smoothed with a third order Savitzky–Golay filter to yield C_A and C_B .¹⁹ Secondly, we add low-pass filtered Gaussian noise ($N_A(\sigma)$ and $N_B(\sigma)$) to these

smoothed curves with a zero mean and varying standard deviation σ . The cut-off frequency of the second order low-pass Butterworth filter was chosen to match the typical time-scale of the experimental noise. The diffusion extraction method is followed based on these smoothed curves with added noise $C_A + N_A(\sigma)$ and $C_B + N_B(\sigma)$ for the different values of σ . The procedure is clarified in Fig. 5. We can then extract how the obtained diffusion coefficient is affected by an increase in experimental noise. The results are shown in Fig. 6. When the applied noise has a standard deviation $\sigma > 0.5 \text{ g L}^{-1}$, the diffusion coefficient is varying rapidly up and down such that a reliable extraction of the diffusion coefficient is no longer possible. We also evaluated the experimental noise of the measured concentration profiles of the microring resonators. For this calculation, we take the standard deviation of the

difference between the Savitzky–Golay smoothed curve and the measured concentration curves of the ring resonators in set 2, 3 and 4 (the resonators that can be used for diffusion extraction). This way we obtain an average standard deviation value of 0.081 g L^{-1} . This value is indicated in Fig. 6 by a green line. The diffusion coefficient that is found based on the smoothed curves ($\sigma = 0$) has a value $16.306 \times 10^{-10} \text{ m}^2 \text{ s}^{-1}$, which is 2.88% lower than the literature value.

8. Conclusion and future outlook

We presented a new method to study the diffusion process of small solutes in microfluidic channels with an integrated optofluidic chip. Both glucose and NaCl were used as example solutes to demonstrate the potential of this method. In the glucose diffusion measurements, we experimented with two distinct cases of mass transport: one where the glucose can enter the diffusion channel from a stopped flow and a second, where the glucose enters from a moving reservoir. In the first case, pure diffusion applies, whereas the latter serves as a text-book example of a driven cavity. In the NaCl diffusion measurements, we used two distinct temperature settings to confirm the increase in diffusion speed with temperature. The robustness of the measurement procedure was investigated. It shows that when the concentration curves are measured with an experimental accuracy σ of up to 0.85 g L^{-1} the error in diffusion coefficient remains lower than 3.0%. The presented method is also robust against temperature variations during the measurements as reference sensors can be employed. It is furthermore versatile in the way the ring resonators are positioned along the microfluidic channels, such that mass transport can be observed over a large chip area. It is important, however, that the distance between the consecutive ring resonators is known. Future improvements include a new silicon-on-insulator chip design with more micro-ring resonators and a smaller ring spacing than 1.8 mm in the diffusion channel. This leads to more and faster acquired time-dependent concentration profiles that can be used in the determination of the diffusion coefficient. In a last step, the whole measurement procedure and data extraction can be automated. This will make way for a quick and accurate diffusion coefficient determination.

Acknowledgements

The authors thank the Flemish agency IWT for financial support through the project SBO GlucoSens as well as the European Research Council through the project InSpectra.

References

- 1 D. Ambrosini, D. Paoletti and N. Rashidnia, *Opt. Lasers Eng.*, 2008, **46**, 852–864.
- 2 J. W. Mares and S. M. Weiss, *Appl. Opt.*, 2011, **50**, 5329.
- 3 C. Culbertson, S. Jacobson and J. M. Ramsey, *Talanta*, 2002, **56**, 365–373.

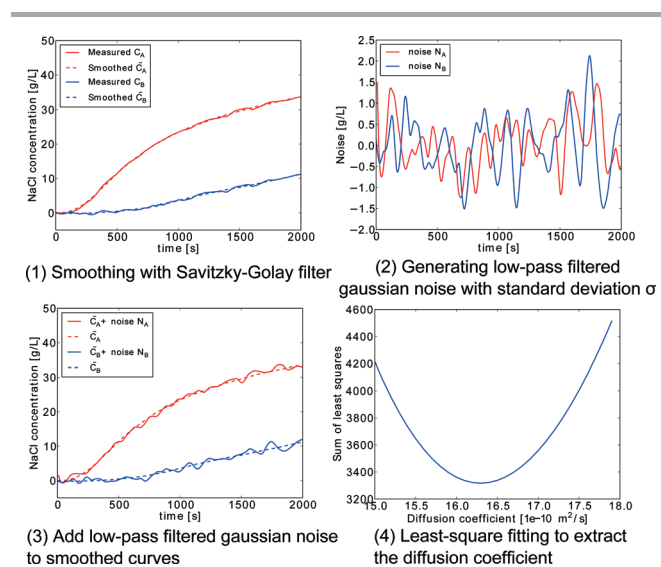


Fig. 5 Step-by-step visualization of the procedure followed to obtain the diffusion coefficient for a given experimental noise with standard deviation σ .

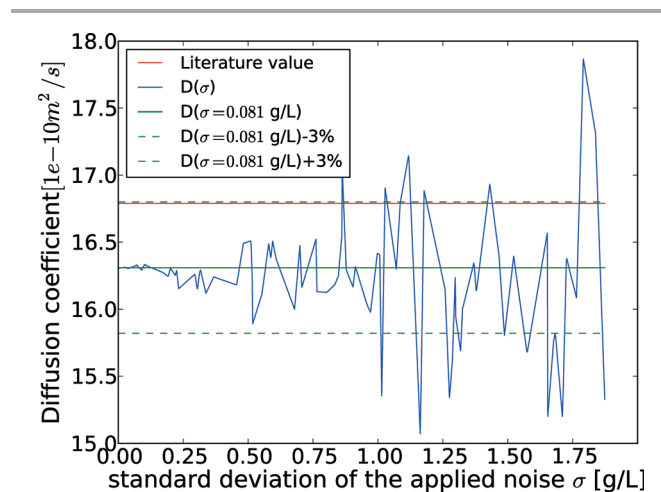


Fig. 6 Extracted diffusion coefficient for a given experimental noise with standard deviation σ (blue). The red line shows the literature value whereas the green line shows the diffusion coefficient D for an experimental noise $\sigma = 0.081 \text{ g L}^{-1}$ and the $D(\sigma = 0.081 \pm 3\%)$ limits.

- 4 A. E. Kamholz, E. A. Schilling and P. Yager, *Biophys. J.*, 2001, **80**, 1967–1972.
- 5 K. De Vos, I. Bartolozzi, E. Schacht, P. Bienstman and R. Baets, *Opt. Express*, 2007, **15**, 7610–7615.
- 6 M. Luchansky, A. Washburn, T. Martin, M. Iqbal, L. Gunn and R. Bailey, *Biosens. Bioelectron.*, 2010, **26**, 1283–1291.
- 7 J. Anderson, D. Chiu, H. Wu, O. Schueller and G. Whitesides, *Electrophoresis*, 2000, **21**, 27–40.
- 8 K. Larin, T. Akkin, R. Esenaliev, M. Motamedi and T. Milner, *Appl. Opt.*, 2004, **43**, 3408–3414.
- 9 W. Bogaerts, P. De Heyn, T. Van Vaerenbergh, K. De Vos, S. Kumar Selvaraja, T. Claes, P. Dumon, P. Bienstman, D. Van Thourhout and R. Baets, *Laser Photonics Rev.*, 2012, **6**(1), 47–73.
- 10 S. K. Selvaraja, P. Jaenen, W. Bogaerts, D. Van Thourhout, P. Dumon and R. Baets, *J. Lightwave Technol.*, 2009, **27**, 4076–4083.
- 11 D. Taillaert, W. Bogaerts, P. Bienstman, T. Krauss, P. Van Daele, I. Moerman, S. Verstuyft, K. De Mesel and R. Baets, *IEEE J. Quantum Electron.*, 2002, **38**, 949–955.
- 12 K. De Vos, J. Girones, T. Claes, Y. De Koninck, S. Popelka, E. Schacht, R. Baets and P. Bienstman, *IEEE Photonics J.*, 2009, **1**, 225–235.
- 13 K. Tang, E. Liao, W. Ong, J. Wong, A. Agarwal, R. Nagarajan and L. Yobas, *J. Phys.: Conf. Ser.*, 2006, 155.
- 14 M. D. J. K. Gladden, *J. Am. Chem. Soc.*, 1953, **75**, 3900–3904.
- 15 W. Zimmerman and B. Hewakandamby, *Microfluidics: history, theory and applications*, 2006, vol. 466, p. 143.
- 16 T. Chiang, W. Sheu and R. Hwang, *Int. J. Numer. Methods Fluids*, 1998, **26**, 557–579.
- 17 *Solute diffusion in Methods of Soil Analysis Part IV*, ed. J. Dane and G. Topp, Soil Science Society of America, 2002.
- 18 J. Kestin, H. E. Khalifa and R. J. Correia, *Tables of the dynamic and kinematic viscosity of aqueous NaCl solutions in the temperature range 20–150 C and the pressure range 0.1–35 MPa*, American Chemical Society and the American Institute of Physics for the National Bureau of Standards, 1981.
- 19 A. Savitzky and M. J. Golay, *Anal. Chem.*, 1964, **36**, 1627–1639.